Polymer 51 (2010) 2244–2254

Contents lists available at ScienceDirect

Polymer

journal homepage: www.elsevier.com/locate/polymer

Forced translocation of polymer chains through a nanotube: A case of ultrafiltration

Ashok K. Das, Po-Da Hong*

Department of Polymer Engineering, National Taiwan University of Science and Technology, Taipei 10607, Taiwan

ARTICLE INFO

Article history:
Received 13 January 2010
Received in revised form
11 March 2010
Accepted 17 March 2010
Available online 25 March 2010

Keywords:
Forced translocation of polymers
Polymer chains through a nanotube

ABSTRACT

Translocation of polymer chains under the application of an external force has been studied through coarse-grained Monte Carlo simulations. The chains are pulled through a nanotube of finite length and diameter and their translocation times measured. The average translocation time, τ follows a scaling relation involving the chain length, N and applied force, F as, $\tau \sim N^{\nu'}F^{-\mu}$, where ν' and μ are two different exponents ($\nu' = 0.674$, and $\mu = 0.95 \pm 0.05$). The scaling law is closely similar to the nanopore translocation scaling law reported by Milchev et al. [Ann N Y Acad Sci 2009;1161:95]. Characteristic signatures of the chain escape time have been exhibited by the square of end-to-end distance R^2, axial radius of gyration R_{g-x} and other constituent properties. The behavior of the linear polymers under the application of a pulling force has been exploited to gain insights into the ultrafiltration process of unentangled polymers in dilute solution. The generic pulling force–translocation time (F, τ) data obtained through simulation can be matched reasonably well with the hydrodynamic force–critical macroscopic flow time (f_h, Q_c^{-1}) data and also with the hydrodynamic force–reduced critical microscopic flow time (f_h, q_c^{-1}) data obtained in the ultrafiltration experiment on long linear polystyrene chains in cyclohexane, as recently reported by Ge et al. [Macromolecules 2009;42:4400] The simulation technique reported here may be extended to study biomolecular transports occurring in long protein channels, as studied experimentally through current–time or voltage–time traces.

1. Introduction

Translocation of polymers/biopolymers through nanopores like those present in cell membranes and semipermeable membranes used in osmosis/reverse osmosis has been an active area of research with the experimentalists as well as theorists. More than a decade ago Kasianowicz et al. [1] first reported the epoch making experiment on characterizing polynucleotide molecules using the α-hemolysin ion channel. This was followed by a variety of experimental evidences using the α-hemolysin ion channel as a detector for RNA segments [2], as an orientation discriminator for DNA [3] and also as a sequence dependent gating of DNA hairpins [4]. These experiments emphasize the importance of nanopores of biological origin. Translocation through such nanopores has been exploited in diverse applications like controlled drug delivery [5], gene therapy [6] and DNA sequencing [7]. Artificial solid state nanopores were also synthesized and successfully exploited to detect single stranded DNA [8]. Asymmetric polymer nanopores prepared by latent ion track-etching technique were proved to be successful in discriminating between DNA fragments of different lengths [9]. Similar technology has also found application in making of alkenyl and alkyl fullerene in carbon nanotubes through which structural and orientational information of single molecules have been obtained [10].

In a recent article, Ge et al. reported the macroscopic flow rate dependence of retention concentration of linear polystyrene of varying molecular weights [11]. The authors raised the question about the magnitude of force needed to make the linear polymers pass through small pores of the ultrafiltration process. The exact force requirement depends on many factors such as state of the polymer (i.e. coiled or blob state), macroscopic flow rate, solution viscosity, temperature and pore size. The importance of nanopores and translocation of biopolymers/polymers through them thus recognized led to theoretical developments [12–16] accompanied by computer simulation [17–20] studies. The first theoretical formalism of polymer translocation through a cylindrical channel has appeared recently [21]. A Gaussian chain without the excluded volume and hydrodynamic interactions, translocating between two spherical compartments, was considered. The average translocation time of the chain was shown to have complex dependence on chain length, channel diameter, channel length and sizes of the donor and receptor compartments. The excluded volume effect was considered for polymer translocation in a short nanochannel

* Corresponding author. Fax: +886 2 27376544.
E-mail address: poda@mail.ntust.edu.tw (P.-D. Hong).

0032-3861/$ – see front matter © 2010 Elsevier Ltd. All rights reserved.
doi:10.1016/j.polymer.2010.03.030

between two containers by Xie et al. [22]. These authors showed that the excluded volume effect significantly alters the polymer translocation time, with a non-monotonic dependence on the length of the chain.

In this article, we particularly focus on the passage of linear polymers through a nanochannel of finite length and diameter, thereby looking more closely into the details of the ultrafiltration process. There is a time delay by which the first monomer of a coiled chain from the bulk suspension finds the mouth (i.e. entry point) of the nanochannel. One may conceive the ultrafiltration as a forced translocation of the polymer coil through the fixed nanochannel, and the translocation time (or escape time) may be defined as the time counted from the entry of the first monomer into the nanochannel to the exit of the last monomer out of the nanochannel. In the simulations, a pulling force along the axial direction acts on the first monomer from the chain's entry to exit from the nanochannel.

We employ a new model, Fraenkel + Lennard-Jones for the linear polymers (the more widely used being the FENE + Lennard-Jones model). The flexible bead-spring chains are then subjected to enter a nanotube of finite length under the application of an external pulling force. In order to gain some insight of the motion of the polymer chain through the nanotube, we monitor the square of the end-to-end distance and the axial and radial radii of gyration of the chain. Further, changes in the chain-entropy inside and outside the nanotube has been manifested by the calculation of the Flory free energy [23]. All these physical properties leave their signatures of the confinement and subsequent release of the polymer chain from the nanochannel. With respect to dependence of average translocation time on pulling force and chain length, we arrive at scaling laws which have been closely similar to those obtained for translocation through nanopores. This establishes the validity of our simulations. Subsequently, we match the simulation data of (pulling force–translocation time) with the ultrafiltration experimental data [11] of (hydrodynamic force–critical macroscopic flow time) and (hydrodynamic force–reduced critical microscopic flow time), with a reasonably good agreement. The question of force requirement for the passage of the linear polymer chains through the nanochannels in an ultrafiltration unit has been answered through the simulations of the near-real linear polymer chains using the generic Fraenkel + LJ potential model considered in this article.

2. Simulation techniques

The polymer chains have been modeled as bead-spring chains of Lennard-Jones (LJ) particles interacting through the Fraenkel potential [24] (for the bead-bead backbone) and the repulsive Lennard-Jones potential (for the non-neighbor beads). The Fraenkel potential has been used earlier [25,26] for the stress relaxation studies on single chains and also for single chains confined in a tube [27]. The potential has a harmonic form

$$U_{\text{Fraenkel}}(r) = \frac{H_F}{2}(r - b_0)^2, \tag{1}$$

where, H_F is the force constant and b_0 is the equilibrium bead–bead distance. The repulsive Lennard-Jones potential has the form

$$U_{LJ}(r) = 4\varepsilon\left[\left(\frac{\sigma}{r}\right)^{12} - \left(\frac{\sigma}{r}\right)^{6}\right] + \varepsilon, \quad r \le (2)^{1/6}\sigma, \tag{2a}$$

$$U_{LJ}(r) = 0, \quad r > (2)^{1/6}\sigma, \tag{2b}$$

where σ is the diameter of a bead and ε is the energy parameter representing the depth of the potential. This form of the LJ potential is also known as the Weeks–Chandler–Andersen (WCA) potential [28]. The excluded volume effect of the polymer has been included in the repulsive LJ potential through the parameter σ. As the neighboring beads interact through the Fraenkel potential, the non-neighbor pairs interact through the LJ potential. Throughout the simulations, we have set $H_F = 400\ k_BT$, $b_0 = 1.0\sigma$ and $\varepsilon = 0.83\ k_BT$, where, k_B is the Boltzmann constant and T is the absolute temperature. The choice of b_0 and ε has been kept the same as was done by Huopaniemi et al. in a two-dimensional simulation study on polymer translocation [18].

It is worthwhile to mention here that we have opted for the Fraenkel + LJ combination as the chain potential over the FENE + LJ combination. Although the latter is more frequently used in polymer simulations, it is asymmetric with respect to the equilibrium bond length ($= 0.96\sigma$) [29]. The Fraenkel + LJ combination does not have any appreciable asymmetry around the potential minimum, as can be seen from the plots in Fig. 1.

Initial configurations of chains of N beads have been generated as follows: Taking the first bead as the seed (placed arbitrarily at the origin), coordinates (x_i, y_i, z_i) of the successive beads are generated using $(x_i = x_{i-1} + \sigma\sin\theta\cos\phi,\ y_i = y_{i-1} + \sigma\sin\theta\sin\phi,\ z_i = z_{i-1} + \sigma\cos\theta,$ for $i = 2, 3, \ldots, N)$; angles θ and φ are obtained from $\theta = \pi^* qq$ and $\phi = 2\pi^* ff$, respectively, where qq and ff are two random numbers generated for each bead. Consecutive inter-bead distances are matched with σ, before accepting the coordinates of the new bead to build the chain. Each such chain has been equilibrated for 10^6 Monte Carlo (MC) steps prior to examining the forced translocation (i.e., entry into the nanotube and subsequent escape). The equilibration of the chains has been monitored through the calculation of the square of end-to-end vector $<R^2>$ and the square of the radius of gyration $\langle R_g^2\rangle$. For each chain length (characterized by N, number of beads in the chain), we monitor the $<R^2>$ and $\langle R_g^2\rangle$ for 100 chains. The average magnitudes of these quantities are given in Table 1. After the equilibration steps, the chain has been relocated such that the first monomer of the chain is placed at the base of the nanotube, located at (0, 0, 0). The translocation of the chain is then followed by applying a pulling force on the first monomer acting along the axial direction of the nanotube.

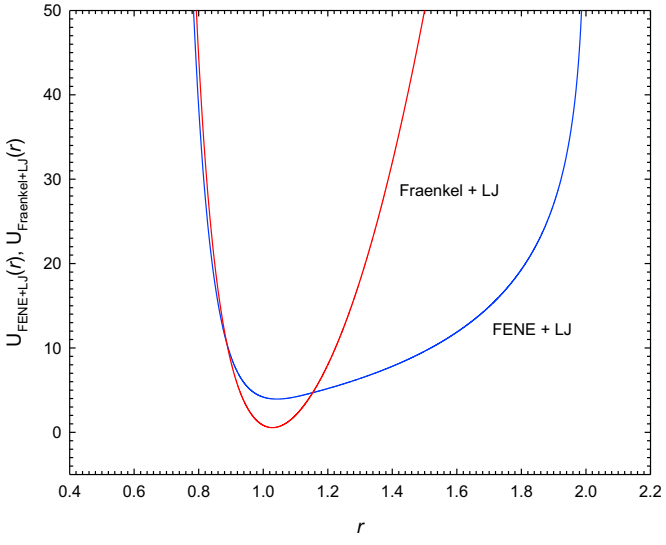

Fig. 1. Comparison of the Fraenkel + LJ and FENE + LJ potential functions. Note the highly asymmetric (with respect to the minimum, at $r = 0.96\sigma$) nature of the FENE + LJ combination as against the near-symmetric Fraenkel + LJ combination (minimum at $r = 1.0\sigma$).

Table 1
Equilibration of the Fraenkel + LJ chains considered for the forced translocation study.

N	$<R^2>/\sigma^2$	$<R_g^2>/\sigma^2$
10	12.5 ± 3.2	1.7 ± 0.4
25	50.1 ± 5.3	4.8 ± 0.4
50	89.9 ± 5.1	12.3 ± 0.8
100	189.5 ± 7.8	18.9 ± 1.1
200	559.5 ± 18.7	41.4 ± 1.5
300	1098.3 ± 51.1	96.5 ± 3.6

$H_F = 400 k_B T$, $b = 1.0\sigma$; $\varepsilon = 0.83 k_B T$. For each value of N, 100 chains were considered.

The physical location of the nanotube is along the $+X$ axis, with the centre of the base at the origin. The cylindrical nanotube has its dimensions as: diameter 1.5σ and length 15σ. As the bead diameter of the monomer is σ, the inner pore of the nanotube ensures that, at any instant of time only a single monomer passes through the cross-section of the tube, when the first monomer of the chain is pulled by applying force. Since the Fraenkel + LJ chain is a string of beads (of diameter σ), the pulling force on monomer no. 1 gets transmitted throughout the chain. It is to be noted that the monomer–monomer bond length ($b_0 = 1.0\sigma$) equals the bead diameter (σ), and hence the pulling force will be experienced by all the monomers of the chain, with a gradient along the chain axis.

Most of the simulation studies on translocation of polymers and biomolecules consider the motion through a 'nanopore'. The nanotube has been considered here in order to mimic the nanochannels in an ultrafiltration unit. For example, a Whatman double-layer membrane has a two-layer structure, the upper thick layer with pore diameter 200 nm (length 59 μm) and a lower thin layer with a smaller pore diameter of 20 nm (length 1 μm) [30]. The nanotube may also be considered as a solid state nanopore [31] whose length is many times larger than the pore diameter. It may also resemble an idealized version of the α-hemolycin ion channel [32]. The interior of the nanotube has reflective characteristics and acts as an impenetrable barrier for the monomers. Once a monomer i is inside the nanotube (characterized by $0 \le x_i \le 15\sigma$) its y- and z-movements are restricted by $-0.75\sigma \le y_i \le +0.75\sigma$; $-0.75\sigma \le z_i \le +0.75\sigma$, where (x_i, y_i, z_i) are the position coordinates of the ith monomer.

In the Langevin dynamics method, motion of each bead i of the chain is dictated by a total force $\mathbf{F}_i^T$ on the bead, which comprises of force arising from potential, frictional force and a random force.

$$\mathbf{F}_i^T = m\ddot{\mathbf{r}}_i = \mathbf{F}_i^C + \mathbf{F}_i^F + \mathbf{F}_i^R, \tag{3}$$

where m is the mass of the bead. The force arising from the chosen Fraenkel + LJ potential are included in $\mathbf{F}_i^C$. The frictional force acting on the bead is $\mathbf{F}_i^F = -\xi \mathbf{v}_i$, where $\mathbf{v}_i$ is the velocity of the bead and ξ is the friction coefficient. The friction coefficient ξ is related to the fluctuations of the random force $\mathbf{F}_i^R$ by the fluctuation–dissipation theorem [33]:

$$\langle \mathbf{F}_i^R(t) \rangle = 0,$$

$$\left\langle \mathbf{F}_i^R(t) \cdot \mathbf{F}_j^R\left(t'\right) \right\rangle = 6 k_B T \xi \delta_{ij} \delta\left(t - t'\right). \tag{4}$$

The temperature of the system being simulated is maintained through Eq. (4). The pulling force is directed along the axis of the nanotube and is expressed as

$$\mathbf{F}_{\text{pull}} = F\hat{x}, \tag{5}$$

where F is the strength of the pulling force exerted on the first monomer of the chain and $\hat{x}$ is a unit vector in the direction of the tube axis. The action of $\mathbf{F}_{\text{pull}}$ is for $0 \le x_i \le 15\sigma$, and it ceases to act once the last bead of the chain leaves the nanotube.

In order to decide the temperature of simulation, we have carried out the following experiment. We consider a 50-bead Fraenkel + LJ chain which has been equilibrated for 10^6 MC steps. The chain was then subjected to forced translocation into the nanotube using a pulling force $F = 1.0$ (in units of $k_B T/\sigma$) acting on the first monomer. Translocation times (τ) at different temperatures were measured by varying ($k_B T/\varepsilon$) for $0.02 \le k_B T/\varepsilon \le 2.0$. The measured τ values at each temperature, shown as points in Fig. 2 are the averages of about 100 simulation runs. Standard deviation in τ is about 1% for $k_B T/\varepsilon > 0.5$ and 3–4% for $0.02 \le k_B T/\varepsilon \le 0.5$. We have also included the curves for the $T^{-2.0}$ and $T^{-1.4}$ dependence [34], for the sake of comparison. It can be seen from the plots that at higher temperatures, $k_B T/\varepsilon > 0.5$, translocation time of the chain remains unchanged while at the lower temperatures, $0.02 \le k_B T/\varepsilon \le 0.5$, the translocation time has a complex temperature dependence. The lower temperature observation is in agreement with that of an $N = 30$ chain considered by Loebl et al. [34]. However, we did not find any increase in τ with T, at higher temperatures. As one of the objectives of the present article is to correlate the (F, τ) data from the simulation with those obtained in the ultrafiltration experiment of Ge et al. [11], we fix the simulation temperature by, $k_B T/\varepsilon = 1.2$ [35]. This choice of simulation temperature is identical to that of Huopaniemi et al. [18], who considered polymer translocation through nanopores.

The interactions between the translocating chains and the nanotube have been modeled as repulsive and have been implemented in the following manner. The interior of the nanotube has reflective characteristics and acts as an impenetrable barrier for the monomers. Thus, the monomers of the chain collide with the interior of the nanotube and get reflected into the tube. The potential energy for such events may be written as, $U_{\text{coll}} = Z_{\text{coll}} \varepsilon_{\text{coll}}$, where Z_{coll} is the number of monomer–nanotube collisions and $\varepsilon_{\text{coll}}$ is the energy exchanged in each such collision. Since σ is the monomer diameter and the diameter of the nanotube is 1.5σ, the

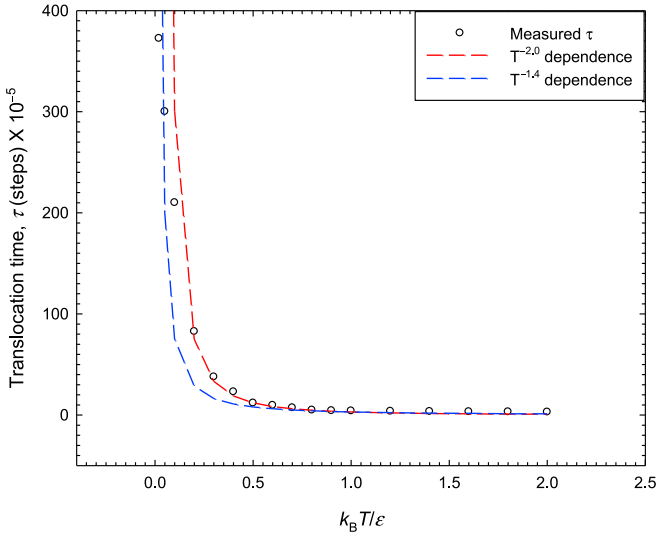

Fig. 2. Variation of translocation time (τ) with simulation temperature (expressed in terms of $k_B T/\varepsilon$) of a 50-bead Fraenkel + LJ chain, under a pulling force $F = 1.0$, acting on the first monomer of the chain. Bead diameter is σ, diameter and length of the nanotube are 1.5σ and 15σ, respectively (see text). The points are the averages of about 100 simulation runs. Standard deviation in τ is about 1% for $k_B T/\varepsilon > 0.5$ and about $3-4\%$ for $0.02 \le k_B T/\varepsilon \le 0.5$. The curves for the $T^{-2.0}$ and $T^{-1.4}$ dependence are also included for the sake of comparison.

chain will experience more number of collisions when pulled using a small force. But when the pulling force is very large, such collisions are expected to be few. For the translocating chain, once a monomer i is inside the nanotube (i.e., $0 \le x_i \le 15\sigma$), the monomer may experience collisions with the interior wall of the nanotube. This will restrict the y- and z-coordinates of the monomer to $-0.75\sigma \le y_i \le +0.75\sigma$; $-0.75\sigma \le z_i \le +0.75\sigma$. The details of the calculations of (x_i, y_i, z_i) for the monomers which collide with the interior of the nanotube during the forced translocation process have been described in the Appendix.

In the Monte Carlo simulation of the Langevin equation of a polymer chain, we replace the continuous time variable with a small time step Δt. If the position of the ith bead at time step t is denoted by $\mathbf{r}_i(t)$, the simulation form of the Langevin equation for the bead can be written as [25,38]

$$\mathbf{r}_i(t+\Delta t)) = \mathbf{r}_i(t) + \frac{d^2}{2k_BT}\mathbf{F}_i^T(t) + \mathbf{d}_i(t), \tag{6}$$

where $\mathbf{F}_i^T(t)$ is the total force on the ith bead (see Eq. (3)) and the random step vector $\mathbf{d}_i(t)$ is characterized by the two moments,

$$\langle \mathbf{d}_i(t) \rangle = 0,$$

$$\left\langle \mathbf{d}_i(t)\mathbf{d}_j\left(t'\right)\right\rangle = d^2\mathbf{I}\delta_{ij}\delta\left(t-t'\right), \tag{7}$$

where, $\mathbf{I}$ is an unit tensor. The random displacement d, and time step Δt, are related through the diffusion constant D, of the chain.

$$d^2 = 2D\Delta t = \frac{2k_BT\Delta t}{\xi}. \tag{8}$$

It is to be noted that in Eqs. (6) and (8), mass of the bead does not appear explicitly as it does in Eq. (3), but the bead mass is implicit in the friction coefficient as, $\xi = k_BT/D = m\gamma$, where γ is the collision frequency [39].

In order to accommodate the entropic effects during the motion of the chain, one can apply the Flory approximation in the stiff limit [40] on the polymer chains (such as those in polymer melts and polyelectrolytes) to calculate the Flory free energy (or conformational free energy), E of the chain [23].

$$\frac{E}{k_BT} = E_{elas} + E_{repl}, \tag{9}$$

where the elastic contribution to the free energy, E_{elas} and the repulsive interaction contribution, E_{repl} are given by

$$E_{elas} \propto \frac{R^2}{l_p\sigma N}, \tag{10a}$$

$$E_{repl} \propto \frac{N^2\sigma^3}{R^3}. \tag{10b}$$

In Eq. (10), $R = \sqrt{\langle R^2\rangle}$ is the root-mean-square end-to-end distance of the chain of N monomers, σ is the monomer diameter and l_p is the persistence length, $l_p = \sigma/p$ (p being the probability of taking a bending step in the self-avoiding walk). Isaacson and Lubensky [41] had used radius of gyration of the polymer instead of end-to-end distance in Eq. (10) to calculate Flory exponent ν for linear and branched polyelectrolytes in dilute solutions. In the simulations, we calculate R in each time step and use Eq. (10) to calculate E_{elas} and E_{repl}.

As the polymer chain is being pulled through the nanotube, its mean radii of gyration along the axial $\langle R_{g-x}\rangle$ and radial $\langle R_{g-yz}\rangle$ directions are different.

$$\langle R_{g-x}\rangle^2 = \left\langle \frac{\sum_{i=1}^{N}(x_i - x_{CM})^2}{N}\right\rangle, \tag{11a}$$

$$\langle R_{g-yz}\rangle^2 = \left\langle \frac{\sum_{i=1}^{N}\left[(y_i - y_{CM})^2 + (z_i - z_{CM})^2\right]}{N}\right\rangle, \tag{11b}$$

where (x_i, y_i, z_i) are the coordinates of the ith monomer and (x_{CM}, y_{CM}, z_{CM}) are the coordinates of the centre of mass of the chain. These two quantities are also being monitored during the motion of the chains in the nanotube.

Throughout this article, we report the results using the following units: length in terms of σ, energy in terms of k_BT, force in terms of (k_BT/σ), and time as the Monte Carlo steps.

3. Results and discussion

After initial generation of the polymer chains, as detailed in Section 2, the equilibration of the chains of varying lengths $N = 10$, 25, 50, 100, 200 and 300 has been monitored for 10^6 Monte Carlo steps, through the calculation of the square of end-to-end vector $<R^2>$ and the square of the radius of gyration $\langle R_g^2\rangle$. The data presented in Table 1 are the averages of 100 chains. The $<R^2>$ and $\langle R_g^2\rangle$ values of the chains in Table 1 clearly indicate that the chains are non-ideal, when tested by the Debye relation [42], $\langle R_g^2\rangle = \langle R^2\rangle/6 = Nb^2/6$, where b is the length of the segment.

We have chosen a Fraenkel + LJ chain with $N = 50$ and a pulling force of $F = 1.0$ to examine the variation of translocation time on temperature. The choice of $F = 1.0$ is such that we should be able to measure the translocation time at the lowest temperature with reasonable accuracy. For this exercise, we report the average τ over 100 runs for each value of (k_BT/ε) for $0.02 \le k_BT/\varepsilon \le 2.0$. The points in Fig. 2 are the measured τ values at each temperature. The standard deviation in τ is about 1% for $k_BT/\varepsilon > 0.5$ and 3 – 4% for $0.02 \le k_BT/\varepsilon \le 0.5$. We have also included the curves for the $T^{-2.0}$ and $T^{-1.4}$ dependence, for the sake of comparison [34]. We observe that at higher temperatures, $k_BT/\varepsilon > 0.5$, translocation time of the chain remains unchanged while at the lower temperatures, $0.02 \le k_BT/\varepsilon \le 0.5$, the translocation time has complex temperature dependence. The lower temperature observation is in agreement with that of an $N = 30$ chain considered by Loebl et al. [34]. It is interesting to note that, for the 50-bead Fraenkel + LJ chain, we did not observe any increase in τ with increasing T (unlike in Ref. [34]), after the decrease of τ at $k_BT/\varepsilon \approx 0.5$, to about 1.2×10^6 MC steps. Our observation is in qualitative agreement with the decrease in flow time with increase in temperature in the ultrafiltration experiment of Ge et al. (in the temperature range 35.80–41.55 °C, the macroscopic flow time decreases from 166.7to 23.5 h, see Table 2) [11]. For $k_BT/\varepsilon > 0.5$, the translocation time for the chain remains practically unchanged. This prompted us to fix the simulation temperature for generating the (F, τ) data for different N (see below) to be, $k_BT/\varepsilon = 1.2$, in line with the nanopore translocation simulation temperature by Huopaniemi et al. [18].

For the generation of the (F, τ) data for different N, we perform the simulation runs on the Fraenkel + LJ chains of varying lengths $N = 10$, 25, 50, 100, 200 and 300, using different pulling forces $F = 0.01$, 0.02, 0.05, 0.1, 0.2, 0.5, 1.0, 2.0, 3.0, 4.0, 5.0, 7.5 and 10.0. Different independent starting configurations have been generated for each of the chains and the results reported are the averages of 50 runs. The standard deviation in τ is about 0.5–1.0% for large force ($F \ge 1.0$) and 6–8% for smaller forces $0.01 \le F \le 0.5$. Fig. 3 displays (not to scale) the different stages of the forced translocation event of a 25-bead Fraenkel + LJ chain.

Table 2
Critical macroscopic flow rate Q_c, reduced critical microscopic flow rate $q_c/k_BT/(3\pi\eta)$ and hydrodynamic force f_h requirement for linear polystyrene chains in cyclohexane above the theta temperature 34.5 °C (From Ref. [11]).

	T (°C)			
	35.80	37.70	39.55	41.55
$Q_c/10^{-2}$ mL h^{-1}	0.60	0.75	1.75	4.25
$q_c/k_BT/(3\pi\eta)/10^{-2}$	0.56	0.72	1.52	3.56
f_h/fN	19	20	38	101
Q_c^{-1}/h mL^{-1}	166.67	133.33	57.14	23.53
$[q_c/k_BT/(3\pi\eta)]^{-1}$	178.57	138.89	65.79	28.09
f_h/N	19×10^{-15}	20×10^{-15}	38×10^{-15}	101×10^{-15}

Critical macroscopic flow time is Q_c^{-1} and reduced critical microscopic flow time is $[q_c/k_BT/(3\pi\eta)]^{-1}$.

In Fig. 4 we present the translocation time (τ) vs. applied force (F) curves for $N = 10$, 25, 50, 100, 200 and 300. For large forces, the translocation time is seen to be linear with respect to the applied force. This observation is as expected [43] and also observed in the simulation of polymer translocation through a 2D nanopore [44]. However, when the pulling force is small, the translocation time is significantly long and the curves for different N are seen to be nearly convergent. From the log–log plot (shown as an inset in Fig. 4), the slopes of the τ vs. F curves are different for different magnitudes of F. Corresponding to the scaling law $\tau \sim F^{-\mu}$, we obtain the values of μ to be 0.95 ± 0.05. This scaling is in agreement with the 2D translocation through a nanopore [44]. However, the scaling law obtained by us for 'nanotube' translocation differs from that for 'nanopore' translocation, reported by Panja and Barkema [45]: $\tau \sim N^{2+\nu}$, for $F = 0$; τ is independent of F, for $FN^{\nu} \leq 1$; and $\tau \sim N^2/F$, for $FN^{\nu} >> 1$, where $\nu = 0.588$, the Flory exponent. We ascribe this discrepancy to the different geometries of the problem; viz. a nanopore has a much smaller thickness in comparison to the length 15σ of the nanochannel, considered in this work. Following Panja and Barkema [45], for unbiased (i.e. with $F = 0$) polymer translocation across a nanopore, the membrane is present as an impenetrable plane across which the chain translocates from the *cis* side to the *trans* side. This translocation gets augmented if a pulling force ($F > 0$) is applied to one end. The chain is pulled so that the central monomer gets tethered at the nanopore; at this instant the pulling force ceases to act, the chain now translocates to the *trans* side and the translocation time is measured. This entails the

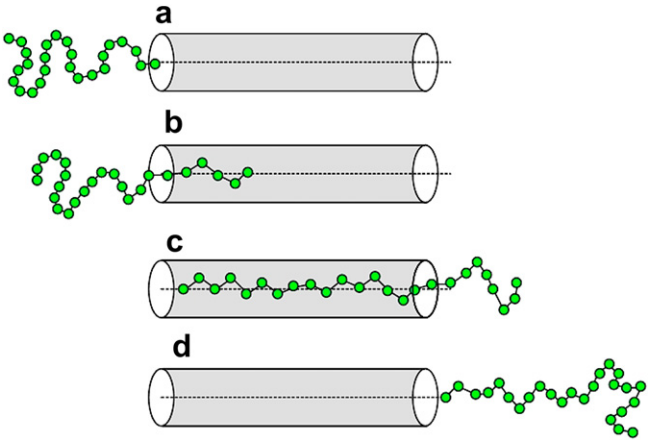

Fig. 3. Different stages of the forced translocation of a 25-bead Fraenkel + LJ chain (not to scale). (a) First monomer about to enter the nanotube; (b) A few monomers already in the nanotube; (c) Polymer chain leaving the nanotube; (d) The chain has just left the nanotube.

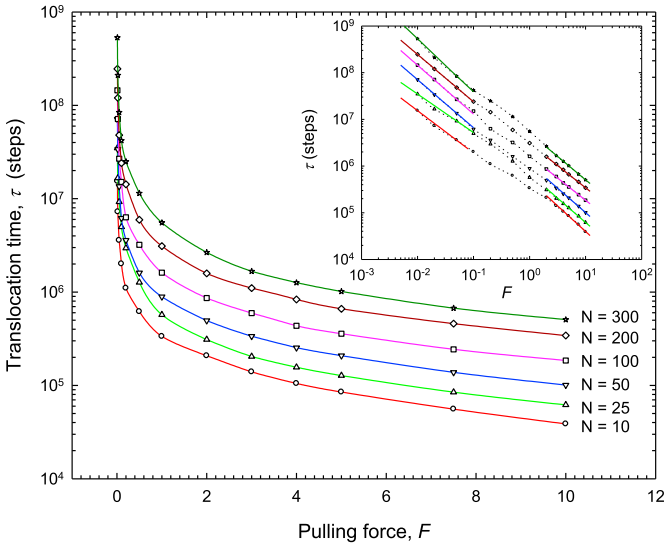

Fig. 4. Translocation time (τ) against the pulling force (F) for linear polymer chains with $N = 10$, 25, 50, 100, 200 and 300 (N is the number of beads comprising the chain). Bead diameter is σ, diameter and length of the nanotube are 1.5σ and 15σ, respectively (see text). The τ values are the averages of 50 runs for each N under different F. The standard deviation in τ is about 0.5 – 1.0% for large force ($F \geq 1.0$) and 6 – 8% for smaller forces $0.01 \leq F \leq 0.5$. The inset shows the log–log plot of the same data, indicating different slopes for different magnitudes of the pulling force.

essential difference between Panja and Barkema's work and the present work, as we do not consider any teethering of the chain and the monomers translocate through the nanotube, unhindered. The action of the pulling force in the 'nanotube' translocation, in our simulations, is from the instant the first monomer enters into the nanotube to the instant when the last monomer leaves the nanotube, without any teethering.

The scaling of the τ vs. N (number of beads) has been shown in Fig. 5 for $F = 0.01$, 0.1, 1.0, 5.0 and 10.0. Considering a model scaling law $\tau \sim N^{\alpha}$, the exponent α has different magnitudes for different forces; for example, $\alpha = 0.6 - 0.7$ at $F = 0.01$ and 0.1. For larger pulling forces, $F = 1.0$, 5.0 and 10.0, the exponent has a larger

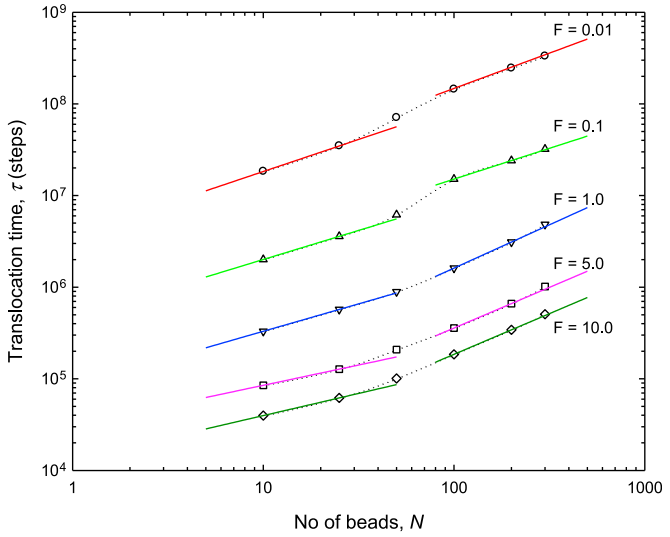

Fig. 5. Translocation time (τ) against the number of beads (N) at five different pulling forces, $F = 0.01$, 0.1, 1.0, 5.0 and 10.0, for $N = 10$, 25, 50, 100, 200 and 300. Data are the same as in Fig. 4. The solid lines are the calculated fits with the scaling relation $\tau \sim N^{\nu'}F^{-\mu}$ using various ν', and $\mu = 0.95 \pm 0.05$.

variation, $\alpha = 0.5–0.6$ for $N < 50$, and $\alpha = 0.8–0.9$ for $N > 100$. This is indicated as the change of slopes of the curves in Fig. 5. We have tested the τ vs. N data using the nanopore scaling law by Panja and Barkema [45] as well as by the nanopore scaling law formulated by Milchev et al. [46]: $t \sim N^{2\nu+1-\gamma_1}/F$, where $\nu = 0.588$ is the Flory exponent and $\gamma_1 = 0.680$ is the *surface entropic exponent*. While the Panja and Barkema scaling law [45] has a fixed expression for different magnitudes of forces, Milchev et al. scaling law [46] may be used by varying γ_1. We find that the data obtained in our simulations match closely the Milchev et al. scaling law [46] with $\gamma_1 = 0.680$ and $\nu' = 0.674$. As the term ν' is about 15% larger in magnitude compared to the Flory exponent for a 3D chain, we may call this ν' to be the quasi-Flory exponent. Thus, although our simulations are done on nanochannel translocation, the polymer translocation times closely follow the nanopore translocation scaling laws, albeit with certain variations.

All the chains simulated have shown distinct signatures of their cylindrical confinement (during the action of the pulling force $\mathbf{F}_{\text{pull}}$, acting on the first monomer of the chain) and subsequent relaxation (when the pulling force has been switched off). These signatures are evident from the plots in the Figs. 6–9, for a 50-bead Fraenkel + LJ chain. In Fig. 6, we show the time evolution of the square of the end-to-end distance, R^2, and the squares of the x-, y- and z-components of the end-to-end vector viz., R_x^2, R_y^2 and R_z^2, respectively. For each of the six forces shown, $F = 0.2$, 0.5, 1.0, 2.0, 5.0 and 10.0, the R^2 and R_x^2 of the chain reach a peak value just before the release of the last monomer from the nanotube. As the pulling force ceases to act from that instant, the chain begins to relax to its equilibrium conformation; hence the square of the end-to-end distance and its x-component start to decrease. This is evident from the plots of R^2 and R_x^2, for all the six pulling forces shown. Since the pulling force on the first monomer acts on the axial (i.e. x-) direction, we do not observe any distinctive escape time feature in the plots of R_y^2 and R_z^2 (lower two panels in Fig. 6). Further, because of the confinement of the chain inside the nanotube ($0 \le x_i \le 15\sigma$), the R_y^2 and R_z^2 components are small in magnitude compared to R_x^2. But, immediately after the chain has fully escaped, the R_y^2 and R_z^2 components start to grow in magnitude with a corresponding decay of the R_x^2 component, ultimately reaching the equilibrium requirement of a free chain: $R_x^2 = R_y^2 = R_z^2 = R^2/3$. This feature can be clearly seen in the bottom two panels in Fig. 6, where both R_y^2 and R_z^2 show the upward trend, after the chain's escape, out of the nanotube. To reach the fully equilibrium state, the chain requires at least one more decade of MC steps, beyond what is shown in the plots.

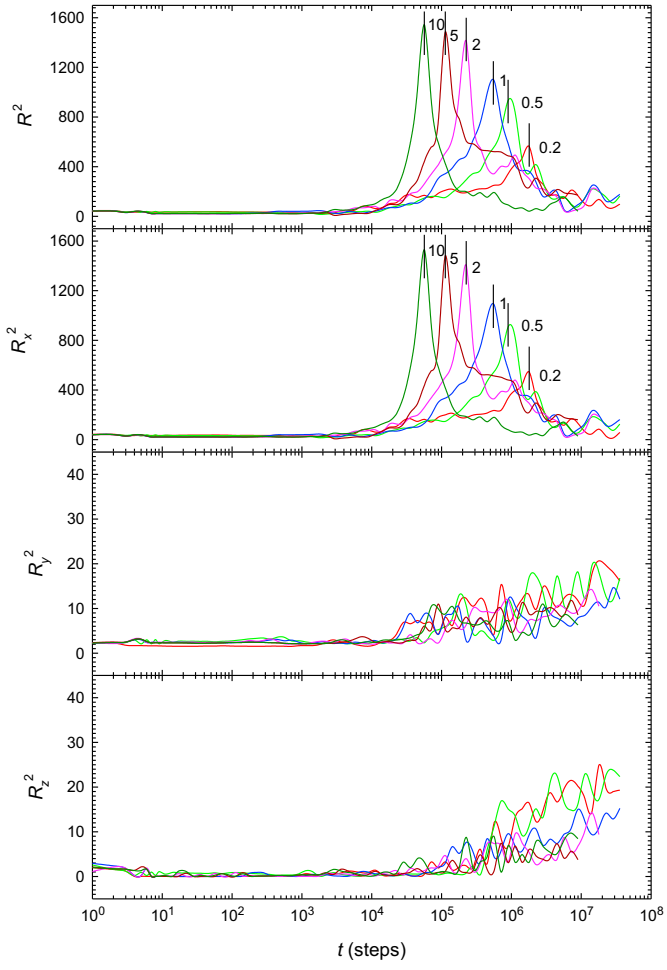

Fig. 6. Time traces of the square of the end-to-end distance, R^2, squares of the x-, y- and z-components of end-to-end vector, R_x^2, R_y^2 and R_z^2, respectively, of a 50-bead chain. The peaks in the R^2 and R_x^2 curves are marked with vertical lines, indicative of the escape times. The numbers by the sides of the curves are the magnitudes of the pulling force F. Plots in Figs. 6–9 relate to the same 50-bead Fraenkel + LJ chain, under different pulling force.

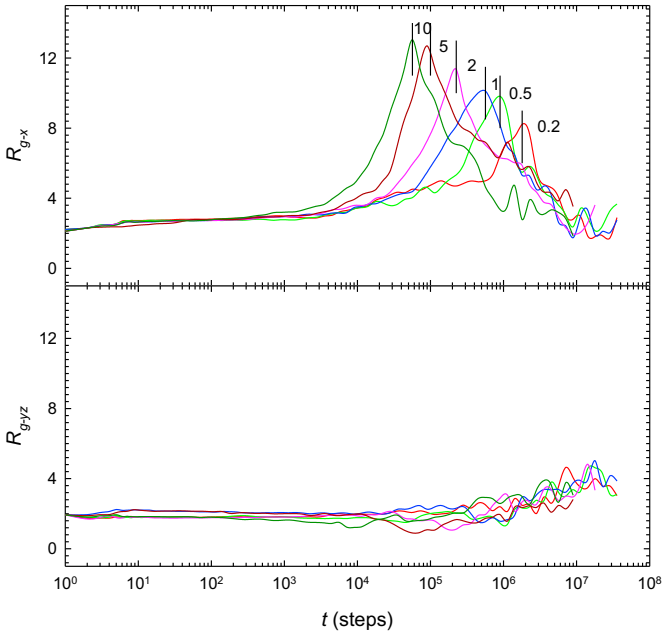

Fig. 7. Axial (R_{g-x}) and radial (R_{g-yz}) radius of gyration of a 50-bead chain. The peaks in R_{g-x} along with the vertical lines are indicative of the escape times. The numbers by the sides of the curves are the magnitudes of the pulling force F.

We have calculated the average radius of gyration along the axial $\langle R_{g-x} \rangle$ and radial $\langle R_{g-yz} \rangle$ directions according to Eq. (11) and these are presented for the 50-bead Fraenkel + LJ chain at six different pulling forces $F = 0.2$, 0.5, 1.0, 2.0, 5.0 and 10.0 in Fig. 7. Similar to the square of end-to-end distance and its x-component, the axial radius of gyration, $\langle R_{g-x} \rangle$ distinctly shows the moments of liberation of the chain out of cylindrical confinement. As expected, the corresponding radial counterpart, $\langle R_{g-yz} \rangle$ does not show such signature escape times, although some dips in the time trace are visible (Fig. 7). As the chain is being pulled along the x-direction, the chain gets elongated along this direction, while any elongation along the radial (i.e. y- and z-) directions is prevented as the monomers must remain confined within the nanotube. The restrictions in the y- and z- movements of the chains while inside

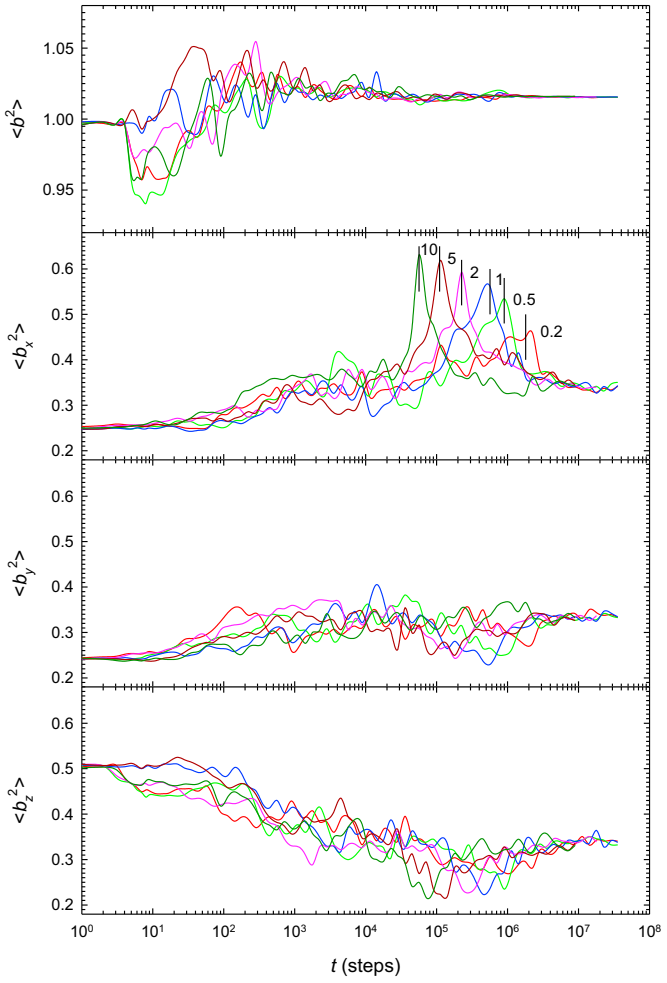

Fig. 8. Time traces of the average square of the bead-bead distance, $<b^2>$, squares of the x-, y- and z-components of bond-segment vector, $< b_x^2 >$, $< b_y^2 >$ and $< b_z^2 >$, respectively, of a 50-bead chain. The time trace of $<b^2>$ exhibits fluctuations around the average value of b_0^2. The vertical lines in the $< b_x^2 >$ plots are indicative of the escape times. The numbers adjacent to the curves indicate the magnitudes of the pulling force F. The differences in the time traces of $< b_y^2 >$ and $< b_z^2 >$ originate from the segment orientation anisotropy, caused by the pulling force and nanotube confinement (see text).

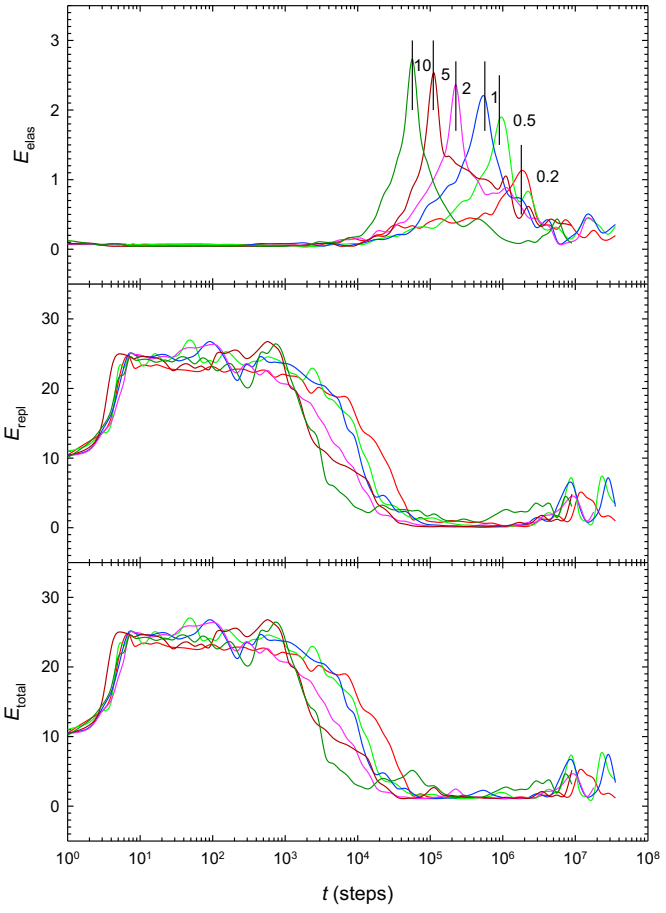

Fig. 9. Elastic (E_{elas}) and repulsive (E_{repl}) contribution of the entropic free energy of a 50-bead chain. The elastic contribution clearly shows the chain escape time signatures. The rest of the legends are the same as in Figs. 6–8. The total entropic free energy E_{total} is shown on the bottom panel. (For interpretation of the references to colour in this figure, the reader is referred to the web version of this article.)

the nanotube have been discussed in Section 2 and also in the Appendix.

Since the elongation of the chain means elongation of the individual bond segments, we observe this phenomenon in the time traces of the function $< b_x^2 >$ (Fig. 8). We recall that $|b| = \sqrt{\langle b^2 \rangle} = \sqrt{\langle b_x^2 + b_y^2 + b_z^2 \rangle}$ where (b_x, b_y, b_z) are the components of the bond-segment vector **b**. The instant the chain escapes from the nanotube (and the pulling force is switched off), the function $< b_x^2 >$ starts to relax back to its average equilibrium value of 0.3377 [26]. As the equilibrium bond length is set as $b_0 = 1$, we observe only fluctuations around 1.013 [26] in the corresponding $<b^2>$ plots. The $< b_x^2 >$ plots clearly indicate the distinctive escape time concomitant to the applied pulling forces $F = 0.2$, 0.5, 1.0, 2.0, 5.0 and 10.0. However, the $< b_y^2 >$ and $< b_z^2 >$ plots shown in the lower panels in Fig. 8 do not exhibit any such distinctive feature indicative of the influence of the pulling force, which is expected, as the pulling force acts along the x-direction of the chain. One may note that the magnitudes of $< b_y^2 >$ and $< b_z^2 >$ are different, for all the applied pulling forces. As the pulling force is tensile in nature, it leads to the development of *orientation anisotropy* in the bond segments. Due to the tensile deformation of the chain, a finite stress results. The stress is directly related to the orientational anisotropy of the segments [47]. The bond-segment orientation anisotropy is further augmented as the chain is confined within the nanotube, interior of which acts as an impenetrable barrier to the monomers. Similar effects due to segment orientation anisotropy were also observed in the simulation of Fraenkel chains under step strain [26].

We now present the entropic free energies of the 50-bead Fraenkel + LJ chain in Fig. 9, calculated using the Flory approximation (Eq. (10)). Since the elastic free energy is directly proportional to the square of the end-to-end distance of the chain (Eq. 10a), the elastic free energy plots follow a pattern similar to that of square of end-to-end distance. The distinctive times of escape from the nanotube have been exhibited by the chain for all of the pulling forces of which only six are shown, viz. $F = 0.2$, 0.5, 1.0, 2.0, 5.0 and 10.0, for the sake of clarity. We show the repulsive and total entropic free energies in the middle and bottom panels, respectively, of Fig. 9. The repulsive free energy has an inverse dependence to the cube of end-to-end distance of the chain (R^{-3} dependence, Eq. (10b)). The repulsive contribution increases to twofold to threefold in magnitude from its initial value, within a few Monte Carlo steps, and remains around this high value, till the first monomer reaches the nanotube end (i.e., $x_1 \geq 15\sigma$). The E_{repl} then starts to decrease as the front part of the escaping chain gets freedom from the confinement (i.e., no y- and z- restriction). A large pulling force makes this decrease in the

E_{repl} earlier in time, compared to that in the case of a smaller force. This is approximately followed by the chain, as can be seen from the middle panel in Fig. 9, the red curve ($F = 0.2$) of E_{repl} decreases later in time while the dark green curve ($F = 10.0$) starts to decrease in early time. Finally, the dominant contribution to the total entropic free energy comes from the repulsive part, as the elastic contribution is much smaller in magnitude ($E_{elas} < 0.1E_{repl}$). This makes the E_{repl} and E_{total} curves look very similar (Fig. 9).

The pulling force–translocation time (F, τ) data presented in Fig. 4 have been matched with the hydrodynamic force–critical macroscopic flow time (f_h, Q_c^{-1}) data and also with hydrodynamic force–reduced critical microscopic flow time (f_h, q_c^{-1}) data of the ultrafiltration experiment [11]. Corresponding to the dilute solution of the linear polystyrene sample ($M_w = 1.8 \times 10^7$ g/mol, $M_w/M_n = 1.06$, $<R_h> = 100$ nm) in Ref. [11], we obtain the number of Rouse segments in the sample to be 3600; as the reported molecular weight of a Rouse segment in a dilute solution is about 5000 [48]. Thus, we match the (f_h, Q_c^{-1}) and (f_h, q_c^{-1}) data of this sample (above the theta temperature, $\theta_c = 34.5$ °C, for polystyrene in cyclohexane, Table 2) with the (F, τ) data obtained by simulation of the $N = 200$ Fraenkel + LJ chain. For the purpose of matching the generic (F, τ) data with the (f_h, Q_c^{-1}) and (f_h, q_c^{-1}) data, we take the largest force, $f_h = 101 \times 10^{-15}$ Newton to be equivalent to $F = 10.0$ (k_BT/σ) of the simulation and the corresponding critical macroscopic flow time, $Q_c^{-1} = 23.53$ h to be equivalent to $\tau = 3.42 \times 10^5$ Monte Carlo steps of the simulation. Such a match is permissible as the bead-spring model of the Fraenkel + LJ chain is a generic model, where each of the physical quantities is expressed in generic units (see Section 2). This type of generic matching has also been reported elsewhere (see Ref. [25], Fig. 10) for the relaxation modulus data of a monodisperse polystyrene sample [25]. Thus, for the $N = 200$ chain, the (F, τ) data in Fig. 4 are transformed into (F^*, τ^*) data, where $F^* = (F \times 101 \times 10^{-15})/10.0$ and $\tau^* = (\tau \times 23.53)/(3.42 \times 10^5)$. As shown in Fig. 10, both the (f_h, Q_c^{-1}) and (f_h, q_c^{-1}) data match reasonably well with the (F^*, τ^*) data, obtained through simulations, emphasizing the validity of the simulations. The macroscopic flow rate (Q) and temperature in the ultrafiltration experiment are controlled with the help of a syringe pump [11], the lowest used flow rate being 0.005 mL/h. One may define the macroscopic flow time as the reciprocal of the corresponding flow rate; physically, macroscopic flow time is the time taken by unit volume (say, 1 mL) of the dilute polymer solution to pass through the nanochannels of the ultrafiltration unit. The microscopic flow rate (q) is defined as the macroscopic flow rate per nanochannel (i.e. $q = Q/n$, where n is the number of pores/channels on each membrane). Thus, the microscopic flow time is the reciprocal of the microscopic flow rate. For the polymer to pass through the nanochannel, the moving monomer of the chain must overcome the hydrodynamic force (f_h) imparted by the solvent and the other monomers. In a dilute solution, the monomer–monomer and monomer–solvent hydrodynamic interactions are quite strong. This makes a moving polymer chain to drag the solvent molecules along with it in bulk and also during its journey through the nanochannel [49]. As the Fraenkel + LJ potential model used in the simulation is a representative of near-real chains with excluded volume, the comparison of the (F^*, τ^*) data with the (f_h, Q_c^{-1}) and (f_h, q_c^{-1}) data of dilute polystyrene above θ_c is meaningful. Above the theta temperature, the excluded volume becomes significant for the polymer [42]. For the ultrafiltration experiment, the monomer size (or blob size) of the linear polymer must be equal to or smaller than the pore size of the nanochannel [11]. This condition has been maintained in the simulations as the bead diameter is σ, and the nanotube

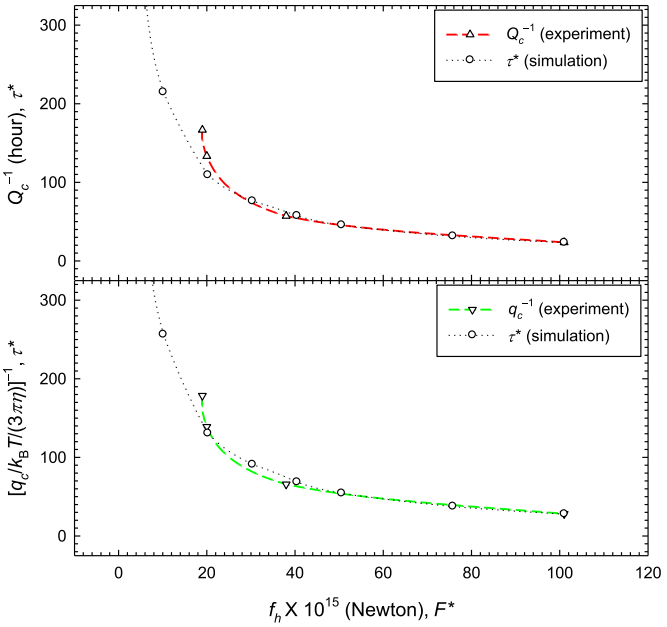

Fig. 10. Simulation vs. experiment [11]. Comparison of the pulling force–translocation time (F, τ) data obtained through simulation with the hydrodynamic force–critical macroscopic flow time (f_h, Q_c^{-1}) data (top panel) and the hydrodynamic force–reduced critical microscopic flow time (f_h, q_c^{-1}) data (bottom panel) obtained in the ultrafiltration experiment [11] on a dilute polystyrene solution (sample $M_w = 1.8 \times 10^7$ g/mol, $M_w/M_n = 1.06$ and corresponds to a 3600-segments Rouse chain). The simulation data are those of a 200-bead Fraenkel + LJ chain (see Fig. 4). The (F, τ) data have been numerically transformed into (F^*, τ^*) in order to match with the (f_h, Q_c^{-1}) and (f_h, q_c^{-1}) data (see text). The lines are drawn to guide the eye.

diameter is 1.5σ. The "bead size" parameter σ can also be considered as "blob size" and in the coarse-grained sense, the simulation results reported here are equally valid when the chain is considered to be "a string of blobs." This explains the good agreement between the (F^*, τ^*) data from numerical simulation with the experimental (f_h, Q_c^{-1}) and (f_h, q_c^{-1}) data, as shown in Fig. 10. The choice of the repulsive form of the LJ potential (Eq. (2)) further justifies the absence of any attractive interaction among the monomers. This negates a poor solvent condition.

4. Conclusions

There is an essential difference between the nanopore translocation and nanochannel translocation. In the nanopore translocation, the linear polymer is pulled through the nanopore so that the monomer at the middle of the chain arrives at the nanopore. The pulling force then ceases to act and the chain has the freedom to translocate to the *trans* side, after attempting a few failed moves to return to the *cis* side. This was incorporated as a memory effect in the chain translocation, by Panja and Barkema [45]. Thus, the scaling law of $\tau \sim N^{2+\nu}$, for $F = 0$; τ is independent of F, for $FN^{\nu} \leq 1$; and $\tau \sim N^2/F$, for $FN^{\nu} >> 1$, where $\nu = 0.588$ is not obeyed by the nanotube translocation of the linear polymers considered here. On the other hand, when the *surface entropic exponent* γ_1 is incorporated into the scaling law, as done by Milchev et al. [46], the scaling law gets modified as $\tau \sim N^{2\nu+1-\gamma}{}_1/F$. The observed nanotube translocation data fit to the scaling relation $\tau \sim N^{\nu'}F^{-\mu}$, where ν' and μ are two different exponents ($\nu' = 0.674$ and $\mu = 0.95 \pm 0.05$). As the nanotube scaling law is closely similar to the nanopore scaling law of Milchev et al. [46], we call the ν' parameter as the quasi-Flory exponent. The physical significance of the surface entropic exponent (γ_1) is that it accommodates the loss of

configurational entropy [49] due to the close proximity of the chain with the nanotube interior (considered to be a solid cylindrical wall with reflective characteristics; see Section 2 and the Appendix). In the present work, the monomer–nanotube interactions are modeled as repulsive. This has been implemented in such a way that, in the event of a collision between a monomer and the nanotube interior, the Langevin position of the monomer gets reflected into the nanotube. Due to such collisions, the chain conformation gets changed during its motion under the applied tensional force. In the case of attractive polymer–nanopore interactions (the monomers getting momentarily adsorbed at the nanopore), the translocation time (τ) of the chain depends on the strength of the interaction and τ has a non-monotonic dependence on this strength [50].

The entry into and escape from the nanotube confinement of the polymer chain have been exhibited by the time traces of its physical properties. (1) The square of the end-to-end distance, R^2 and its x-component, R_x^2 reach a peak value at the instant the last monomer leaves the nanotube. This has been seen in all the thirteen pulling force values we have experimented on. For the sake of clarity, we have shown only six of these in Fig. 6. We observe the escape time characteristics in the time traces of R^2 R_x^2 since the pulling force acting on the first monomer is a tensional force along the x-direction. It is quite natural that these signatures are not seen in the R_y^2 and R_z^2 plots (Fig. 6). (2) The escape time signatures are also evident from the axial radius of gyration, R_{g-x} (Fig. 7), square of the x-component of the bond-segment vector, $\langle b_x^2 \rangle$ (Fig. 8) and the elastic contribution of the entropic free energy, E_{elas} (Fig. 9) plots. The axial radius of gyration, R_{g-x} (along the x-direction of the nanotube) reaches a maximum value (Fig. 7) concomitant with that of the square of the end-to-end distance, R^2. Since the radial radius of gyration, R_{g-yz} (along the radial direction of the nanotube) is practically unaffected by the tensional force along the x-direction, this does not show the characteristic feature. (3) The x-component of the bond-segment vector gets elongated with the application of the pulling force, hence we see the characteristic escape time peak maximum in the $\langle b_x^2 \rangle$ plots (Fig. 8). The $<b^2>$ plots do not show this, as the average bond distance between the beads needs to be maintained around the set value of $b_0 = 1$. This necessitates that the elongation in $\langle b_x^2 \rangle$ must be compensated by a shortening in $\langle b_y^2 \rangle$ and $\langle b_z^2 \rangle$ (Fig. 8). The unequal magnitudes of $\langle b_y^2 \rangle$ and $\langle b_z^2 \rangle$ have been attributed to the fact that orientation anisotropy in the bond segments gets generated within the polymer chain, with the application of the tensional force, and also due to confinement. Such bond-segment orientation anisotropy was also observed while simulating the Fraenkel chains under step strain [26]. (4) The elastic contribution of the entropic free energy, E_{elas} of the chain exhibits the characteristic escape time peaks, since, E_{elas} has a direct dependence on the square of the end-to-end distance, R^2 (Eq. (10)). The repulsive contribution, E_{repl} has a R^{-3} dependence, and it increases to twofold to threefold in magnitude from its initial value, within a short time when the first monomer is pulled into the nanotube. E_{repl} remains around this high value, till the first monomer reaches the nanotube end (i.e., $x_1 \geq 15\sigma$), and then starts to decrease. This is attributed to the fact that the front part of the escaping chain gets freedom from the nanotube confinement, and a large pulling force makes this decrease in the E_{repl} earlier in time. This has been observed from the plots in Fig. 9, where E_{repl} takes the longest time to decrease for the smallest pulling force $F = 0.2$ shown. After the chain escape, this contribution decreases as the chain starts to relax to its equilibrium conformation.

With respect to the ultrafiltration experiment, we are able to quantify the force needed to drag the linear polymer out of the nanotube by considering the variation of the length of the chain, under the assumption that the chain behaves as a coil. The reasonably well-matching of the (F^*, τ^*) data from numerical simulation with the experimental (f_h, Q_c^{-1}) and (f_h, q_c^{-1}) data of the dilute polystyrene solution above θ_c (for the polystyrene sample, $M_w = 1.8 \times 10^7$ g/mol, $M_w/M_n = 1.06$, $<R_h> = 100$ nm) in Fig. 10, justifies the acceptability of the simulations to mimic the ultrafiltration experiment. The requirement that the monomer size (or blob size) must be equal or smaller than the pore size of the nanochannel, has been maintained in the simulations. The excluded volume effect, important in dilute solutions above the theta temperature, has also been an important criterion in choosing the Fraenkel + LJ potential model to describe the near-real chains. In the case of a blob chain, the pore size needs to be increased. Alternatively, if the pore size is kept approximately that of a monomer size, the chain needs to uncoil first before passing through the nanochannel, which naturally increases the time needed for uncoiling followed by dragging out the chain.

It is worthwhile to explore the behavior of the Fraenkel + LJ chains in a nanochannel like that in α-hemolycin, where the channel dimensions are uneven (opening diameter 2.6 nm, followed by an internal vestibule of diameter 3.6 nm, followed by a narrow aperture of 1.5 nm and the end diameter of the pore is 2.2 nm) [4,32]. Although it is quite challenging to formulate an appropriate dynamics of the chain inside such an irregularly shaped nanochannel, the pioneering report by Matthai and Loebl [51] on DNA segments across an α-hemolycin channel highlights the power of the Monte Carlo simulations to relate to the experimental findings [1,52].

Acknowledgements

The authors thank the National Science Council (NSC), Taiwan for financial assistance through Grant No. NSC98-2923-M-011-002-MY2. The computations were performed at the National Taiwan University of Science and Technology (NTUST), Taipei and also at the National Centre for High Performance Computing (NCHC), Hsinchu, Taiwan. We acknowledge both the service providers for this generosity. We record our appreciation for the assistance received from Mr. Bony in the preparation of Figs. 3 and A.1. Finally we thank one of the reviewers for drawing our attention to Ref. [51].

Appendix

The position of each monomer of the polymer chain can be calculated following the Langevin equation (Eq. (6)). The random step vector $\mathbf{d}_i(t)$ for the ith monomer in Eq. (6) may place the monomer outside the nanotube, but the interior wall of the nanotube must reflect the monomer into the tube. Hence in such cases, we need to calculate the reflected position of the monomer so that the chain undergoes translocation through the nanotube for $0 \leq x_i \leq 15\sigma$. The illustrations in Fig. A.1 would be helpful in working out the position coordinates of such monomers.

Fig. A.1(a) considers the case of the first bead of the chain. Its Langevin position is **1**, characterized by (x_1, y_1, z_1). The neighboring bead **2** (x_2, y_2, z_2) is inside the nanotube. Thus, bead **1** needs to be reflected back into the inside, so that its real position is **1'** (x_1', y_1', z_1'). The nanotube is located along the x-axis, with its base centred at the origin (0, 0, 0). From simple geometric considerations, we can write:

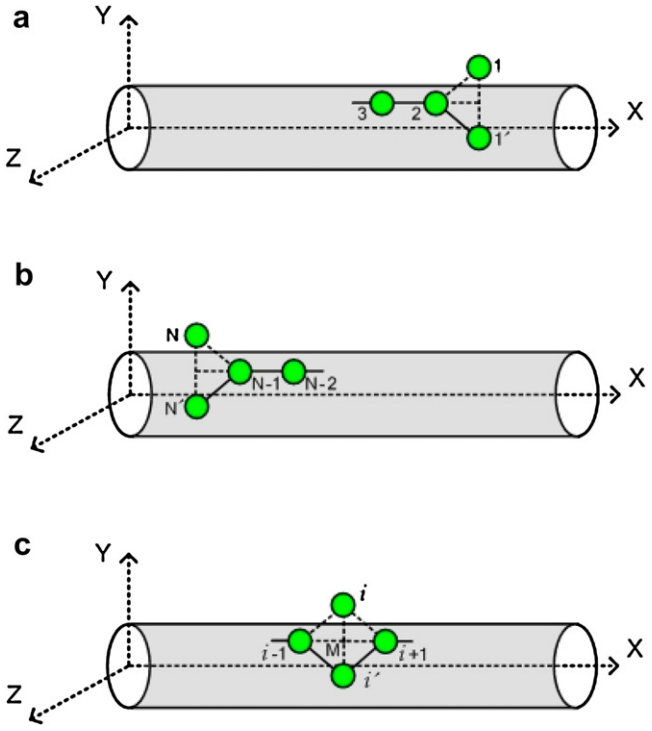

Fig. A.1. Illustration of the nanotube–polymer chain collision (not to scale). (a) The first monomer of the chain collides with the interior of the nanotube and its Langevin position **1** is reflected into position **1′**; (b) The tail monomer of the chain collides with the interior of the nanotube and its Langevin position **N** is reflected into position **N′**; (c) An interior bead of the chain gets reflected into the nanotube, its Langevin position **i** is reflected into position **i′**. **M** is the location of the midpoint of the beads **(i − 1)** and **(i + 1)** (see text).

$$x_1' = x_1,$$

$$y_1' = y_2 - (y_1 - y_2) = (2y_2 - y_1), \tag{A.1}$$

$$z_1' = z_2 - (z_1 - z_2) = (2z_2 - z_1).$$

The transformation can be summarized by the following matrix form:

$$\begin{bmatrix} x_1' \\ y_1' \\ z_1' \end{bmatrix} = \begin{bmatrix} 1 & 0 & 0 & 0 & 0 & 0 \\ 0 & -1 & 0 & 0 & 2 & 0 \\ 0 & 0 & -1 & 0 & 0 & 2 \end{bmatrix} \begin{bmatrix} x_1 \\ y_1 \\ z_1 \\ x_2 \\ y_2 \\ z_2 \end{bmatrix}. \tag{A.2}$$

The reflection of the tail monomer (bead no **N**) has been shown in Fig. A.1(b). The Langevin position is **N**, characterized by (x_N, y_N, z_N). The neighboring bead is **N − 1** with coordinates (x_{N-1}, y_{N-1}, z_{N-1}), is inside the nanotube. When this tail bead is reflected back into the inside, its real position becomes **N′** (x'_N, y'_N, z'_N). As before, from plane geometry we have the following transformation:

$$\begin{aligned} x_N' &= x_N, \\ y_N' &= y_{N-1} - (y_N - y_{N-1}) = (2y_{N-1} - y_N), \\ z_N' &= z_{N-1} - (z_N - z_{N-1}) = (2z_{N-1} - z_N). \end{aligned} \tag{A.3}$$

In the matrix form, the transformation is

$$\begin{bmatrix} x_N' \\ y_N' \\ z_N' \end{bmatrix} = \begin{bmatrix} 0 & 0 & 0 & 1 & 0 & 0 \\ 0 & 2 & 0 & 0 & -1 & 0 \\ 0 & 0 & 2 & 0 & 0 & -1 \end{bmatrix} \begin{bmatrix} x_{N-1} \\ y_{N-1} \\ z_{N-1} \\ x_N \\ y_N \\ z_n \end{bmatrix}. \tag{A.4}$$

The illustration of an interior bead ***i*** of the chain getting reflected into the nanotube has been shown in Fig. A.1(c). In this case, the position coordinates of the reflected bead ***i′*** may be calculated in terms of the coordinates of the midpoint ***M*** of the two neighboring beads (***i − 1***) and (***i + 1***).

Thus we have

$$\begin{aligned} x_i' &= x_i, \\ y_i' &= y_M - (y_i - y_M) = (2y_M - y_i) = (y_{i-1} - y_i + y_{i+1}), \\ z_i' &= z_M - (z_i - z_M) = (2z_M - z_i) = (z_{i-1} - z_i + z_{i+1}), \end{aligned} \tag{A.5}$$

where

$$x_M = 0.5(x_{i-1} + x_{i+1}), \quad y_M = 0.5(y_{i-1} + y_{i+1}), \quad z_M = 0.5(z_{i-1} + z_{i+1}).$$

The corresponding matrix form of the transformation is

$$\begin{bmatrix} x_i' \\ y_i' \\ z_i' \end{bmatrix} = \begin{bmatrix} 0 & 0 & 0 & 1 & 0 & 0 & 0 & 0 & 0 \\ 0 & 1 & 0 & 0 & -1 & 0 & 0 & 1 & 0 \\ 0 & 0 & 1 & 0 & 0 & -1 & 0 & 0 & 1 \end{bmatrix} \begin{bmatrix} x_{i-1} \\ y_{i-1} \\ z_{i-1} \\ x_i \\ y_i \\ z_i \\ x_{i+1} \\ y_{i+1} \\ z_{i+1} \end{bmatrix}. \tag{A.6}$$

References

[1] Kasianowicz JJ, Brandin E, Branton D, Deamer DW. Proc Natl Acad Sci U S A 1996;93:13770.
[2] Akenson M, Branton D, Kasianowicz JJ, Brandin E, Deamer DW. Biophys J 1999;77:3227.
[3] Bates M, Burns M, Meller A. Biophys J 2003;84:2366.
[4] DeGuzman VS, Lee CC, Deamer DW, Vercoutere WA. Nucleic Acids Res 2006;34:6425.
[5] Robinson JR, Lee VH, editors. Controlled drug delivery: Fundamentals and applications. 2nd ed. New York: Marcel Dekker Inc; 1987 (revised and expanded).
[6] Chang DC. Guide to electroporation and electrofusion. New York: Academic Press; 1992.
[7] Turner SWP, Calodi M, Craighead HG. Phys Rev Lett 2002;88:128103.
[8] Fologea D, Gershow M, Ledden B, McNabb DS, Golovchenko JA, Li J. Nano Lett 2005;5:1905.
[9] Mara A, Siwy Z, Trautmann C, Wan J, Kamme F. Nano Lett 2004;4:497.
[10] Koshino M, Solin N, Tanaka T, Isobe H, Nakamura E. Nat Nanotechnol 2008;3:595.
[11] Ge H, Jin F, Li J, Wu C. Macromolecules 2009;42:4400.
[12] Sung W, Park PJ. Phys Rev Lett 1996;77:783.
[13] Muthukumar M. J Chem Phys 1999;111:10372.
[14] Muthukumar M. Phys Rev Lett 2001;86:3188.
[15] Kantor Y, Kardar M. Phys Rev E 2004;69:021806.
[16] Chatelain C, Kantor K, Kardar M. Phys Rev E 2008;78:021129.
[17] Lubensky DK, Nelson DR. Biophys J 1999;77:1824.
[18] Huopaniemi I, Luo K, Nissila TA, Ying SC. J Chem Phys 2006;125:124901.
[19] Panja D, Barkema GT, Ball RC. J Phys Condens Matter 2007;19:432202.
[20] Dubbeldam JLA, Milchev A, Rostiashvili VG, Vilgis TA. Phys Rev E 2007;76:010801[R].
[21] Wong CTA, Muthukumar M. J Chem Phys 2008;128:154903.
[22] Xie Y, Yang H, Yu H, Shi Q, Wang X, Chen J. J Chem Phys 2006;124:174906.
[23] Nakanishi H. J Physique 1987;48:979.

[24] Fraenkel GK. J Chem Phys 1952;20:642.
[25] Lin YH, Das AK. J Chem Phys 2007;126:074902.
[26] Lin YH, Das AK. J Chem Phys 2007;126:074903.
[27] Sheng YJ, Wang MC. J Chem Phys 2001;114:4724.
[28] Weeks D, Chandler D, Andersen HC. J Chem Phys 1971;54:5237.
[29] Bulacu M, van der Giessen E. J Chem Phys 2009;131:064904.
[30] Jin F, Wu C. Phys Rev Lett 2006;96:237801.
[31] Storm AJ, Storm C, Chen J, Zandbergen H, Joanny JF, Dekker C. Nano Lett 2005;5:1193.
[32] Gouaux EJ. Struct Biol 1998;121:110.
[33] McQuarie DA. Statistical mechanics. New York: Harper and Row; 1976.
[34] Loebl HC, Randel R, Goodwin SP, Matthai CC. Phys Rev E 2003;67:041913.
[35] Moreover, we have explored for the temperature range over which a chain is essentially in a good solvent. For this purpose, the 50-bead Fraenkel + LJ chain has been examined (without the nanotube) for the temperature range $0.02 \leq k_BT/\varepsilon \leq 2.0$, by calculating the static structure function $S(q)$ for the chain [36,37]: $S(q) \propto q^{-1/\nu}$ for, $2\pi/\langle R^2\rangle^{1/2} \leq q \leq 2\pi/\sigma$, where, q is the scattering vector, ν is the Flory exponent, R is the end-to-end distance and σ is the monomer diameter. The structure factor scaling law is obeyed by the $N = 50$ chain corresponding to a value of $\nu = 0.34$–0.41 for $0.02 \leq k_BT/\varepsilon \leq 0.1$; $\nu = 0.5$ for $0.2 \leq k_BT/\varepsilon \leq 0.5$; and $\nu = 0.625$ for $0.6 \leq k_BT/\varepsilon \leq 2.0$. Thus the poor solvent ($\nu < 0.5$), θ-solvent ($\nu = 0.5$) and good solvent ($\nu = 0.59$) conditions for the $N = 50$ chain have been established. This further justifies our choice of the simulation temperature, $k_BT/\varepsilon = 1.2$.
[36] Grest GS, Kremer K. Phys Rev A 1986;33:3628.
[37] Maurice RG, Matthai CC. Phys Rev E 1999;60:3165.
[38] Leach AR. Molecular modelling: principles and applications. 2nd ed. Essex: Pearson Education Limited; 2001.
[39] We note that the frictional force is proportional to the speed of the particle, $\mathbf{F}^{\text{friction}} = -\xi\mathbf{v}$, where $\mathbf{v}$ is the velocity of the particle (or, bead) and ξ is the friction coefficient. The friction coefficient (ξ) is related to the collision frequency (γ) by $\gamma = \xi/m$, where, m is the mass of the particle. The quantity γ^{-1} can be considered as the time taken by the particle to lose memory of its initial velocity (or, γ^{-1} is the velocity relaxation time of the particle) (Ref. [38], p. 388–389). Therefore, Eqs. (6) and (8) are not in conflict with Eq. (3) as the friction coefficient ξ contains the implicit dependence on mass, m. One may rewrite Eq. (6) as

$$\mathbf{r}_i(t+\Delta t) = \mathbf{r}_i(t) + \frac{\Delta t}{\zeta}\mathbf{F}_i^{\mathrm{T}}(t) + \mathbf{d}_i(t) = \mathbf{r}_i(t) + \frac{\Delta t}{\gamma m_i}\mathbf{F}^{\mathrm{T}}(t) + \mathbf{d}_i(t) \tag{6'}$$

When the velocity relaxation time (γ^{-1}) is much smaller than the integration time step (Δt), the motion is diffusive, and the interparticle force is assumed to be constant over Δt (see also Eqs. (7.121) in Ref. [38]).
[40] Flory PJ. Statistical mechanics of chain molecules. New York: Wiley; 1969.
[41] Isaacson J, Lubensky TC. J Physique 1980;41:L-469.
[42] Rubinstein M, Colby RH. Polymer physics. New York: Oxford University Press; 2003.
[43] Luijten E, Cacciuto A. Comput Phys Comm 2007;177:150.
[44] Huopaniemi I, Luo K, Nissila TA, Ying SC. Phys Rev E 2007;75:061912.
[45] Panja D, Barkema GT. Biophys J 2008;94:1630.
[46] Milchev A, Dubbeldam JLA, Rostiashvili VG, Vilgis TA. Ann NY Acad Sci 2009;1161:95.
[47] Doi M. Introduction to polymer physics. Oxford: Clarendon Press; 1996. p. 55.
[48] Inoue T, Uematsu T, Osaki K. Macromolecules 2002;35:820.
[49] Marenduzzo D, Orlandini E. Europhys Lett 2006;76:519.
[50] Chen YC, Wang C, Zhou YL, Luo MB. J Chem Phys 2009;130:054902.
[51] Matthai CC, Loebl H. Adv Sci Technol 2004;44:337.
[52] Meller A, Nivon L, Branton D. Phys Rev Lett 2001;86:3435.